CHARACTERIZATION OF PLANT BASED ORGANIC DYE MIXTURES FOR DYE SENSITIZED SOLAR CELLS (DSSCS) APPLICATIONS.

Abstract

Aims/ objectives: To extract (solvent extraction process) and mix chlorophyll and anthocyanin dye pigments at varying concentration percentages. To study optical characterisation (absorption and transmission) of the varying concentration percentages of the dye mixtures in (1) To fabricate dye-sensitised solar cells (DSSCs) from the varying concentration percentages of the dyes in (1). To study I-V characteristics of the fabricated dye sensitized solar cells (DSSCs) in (3).
Study design: Experimental.
Place and Duration of Study: Department of Mathematics and physical sciences, Maasai Mara University, between September 2024 and March 2025.
Methodology: Different natural dye mixtures, extracted from *Spinacia oleracea* (spinach leaves) and *Bougainvillaea glabra* (red bougainvillaea flower) to obtain the two pigments, chlorophyll and anthocyanin respectively, were blended together at differnt ratios, to establish a mixture with optimum properties and highest efficiency for application in DSSCs. The dye-sensitised solar cell was fabricated where the compact layer was made through spray pyrolysis, followed by depositing TiO_2 paste through spin coating on top of the compact layer, and then the coated TiO_2 glass electrodes were immersed in dyes mixtures solution for dye pigment to adsorb on TiO_2 nanoparticles. Thereafter a counter electrode with two drilled holes was fused together, and electrolyte was fed through the drilled holes. The mixtures and the fabricated DSSCs were characterized using UV-VIS spectroscopy and the Solar Cell I-V Test System respectively.
Results: Dye sample solutions of chlorophyll and anthocyanin were extracted via solvent extraction, filtered and then mixed in different ratios. The plant products used were analysed to check if they had the required pigments (chlorophyll and anthocyanin). The dilution of the known concentrated dye to different solution concentrations was done, and their absorbance characteristic were determined. The absorbance data of the ruthenium dyes showed the highest absorbance values within the visible light region at 437 nm, and the absorbance of the unknown solutions was determined at the same wavelength of 437 nm. The transmittance of the dye mixtures about the standard solution of commercial ruthenium complex dye was determined, where ruthenium had the least transmittance, indicating that it permits less amount of light to penetrate past the dye within the visible light region. Furthermore, the dye absorption curves were determined by the UV-VIS spectrophotometer, which showed that mixing chlorophyll and anthocyanin increases the range of light absorption. The optical characterization of the annealed thin films was done, and the transmittance spectra for the two layer and annealed TiO_2 films displayed a gradual increase in transmittance within the visible light range, indicating that visible light transmits very well through the film which is an excellent feature for solar cells in harvesting visible light from sun. The film thickness of the annealed compact and TiO_2 layer were determined using a DEKTAK- Profilometer. Compact layer size and its effect on the functionality of the DSSC was determined. Current-voltage (I-V) Characteristics of the DSSC were determined at room temperature to determine the effects of Chlorophyll and anthocyanin dyes on the DSSC's ability to harvest visible light. It was found out that pure anthocyanin dye led to higher efficiency compared to all other dyes since it has a wider spectrum range for absorbing visible light and chlorophyll had the lowest absorption spectrum range of visible light hence the lowest cell efficiency. Furthermore, mixtures' efficiencies depend on the amount of anthocyanin present, and thus higher quantity of anthocyanin leads to higher efficiency compared to chlorophyll.
Conclusion: Transmittance and absorbance characteristics of the fabricated DSSC assisted in establishing the amount of light the dye mixture absorbed. Electrical characterization, such as I_SC, V_OC, and PM, was calculated at room temperature. This research emphasized on investigating the properties of different dyes mixtures and came up with a mixture of the best properties.

Keywords: Solvent-extraction; Chlorophyl; Anthocyanin; Dye; Spin-coating; Spray-pyrolysis; Transmittance; Absorbance

1 Introduction

Recently, there has been high demand of electricity for domestic and industrial applications Muñoz-García et al., 2021. Fossil fuels, being the main source of energy, have some drawbacks such as being environmentally unfriendly, expensive, and exhaustible Sekaran and Marimuthu, 2024. Fuels such as coal, crude oil, and natural gas are getting depleted at a high rate, thus creating great concern for the search of renewable sources of energy. Furthermore, they are also environmentally non-conducive substances Sugathan et al., 2015. Combustion of fossil fuels gives out harmful gases which in turn cause air pollution. This air pollution causes adverse effects of climate change, such as the greenhouse effect.

Owing to the above reasons, there has been increased interest in the search for alternative but sustainable sources of energy that are environmentally friendly Badawy et al., 2024. Solar energy has been the preferred alternative as it's renewable, clean, green, and cost-effective Sekaran and Marimuthu, 2024. There are three types of solar cell generations, namely: first solar cell generation, second solar cell generation, and third solar cell generation. The third generation solar cells are mainly the Dye Sensitized Solar Cells (DSSCs) Parasuraman and Ramakrishnan, 2023. Third-generation solar cells have a relatively low efficiency compared to other generations Sugathan et al., 2015. Though the efficiency is relatively low compared to other solar cells in the market, they are cheaper to fabricate since they use locally available materials Sekaran and Marimuthu, 2024. Furthermore, they have promising ideas of improvement of efficiency through proper and compact designing Badawy et al., 2024. Currently, many researchers are utilizing different technologies to improve the efficiency of DSSCs Saud et al., 2024. For example, the use of different dyes to determine the best dye in terms of photon absorption Lin et al., 2025. These are some of the promising ideas that researchers are dwelling on to come up with the best dye to be used and have the best electron generation.

The process of photo-generated electrons and their recombination at the counter electrode and electrolyte has shown characteristic efficiency decrement Khan et al., 2023. This is mainly caused by the nature of bonding of the electrolyte and the counter electrode. This creates a research gap on how and which metal-electrolyte combination is efficient. Also, metal oxide semiconductor material has not been fully explored to determine the best metal oxide Kokkonen et al., 2021. DSSCs have gained much interest because they seek to explore the properties of each material that makes up the composite cell Iqbal et al., 2019. This study investigated different dyes mixtures and their properties to establish the best dye sensitizer to improve cell properties and performance. The mixtures were from chlorophyll dye and anthocyanin dye blended at different concentration percentages Pirdaus et al., 2024.

2 Materials and Methods

2.1 Materials

Transparent conducting oxide (anode), FTO, TiO_2 paste, extracted organic dyes (chlorophyll and anthocyanin), titanium diasopropoxide, acetylacetone, ethanol, iodide/triiodide electrolyte (I-/I-3), transparent conducting glass (Counter electrode), Platisol containing platinum element, Magnetic stirrer, oven/furnace, blender, beakers, thermometer, UV – VIS spectrophotometer, ALPHA step Profilometer, Solar simulator, and a Spray pyrolysis machine.

2.2 Methods

2.2.1 Cleaning of Fluorine-Doped Tin Oxide (FTO) Glass Substrates

One hundred transparent conducting glass substrates (fluorine-doped tin oxide (FTO) Pilkington Tec 15, 15 Ω/sq.) with dimensions of 2 cm $\times$ 2 cm $\times$ 0.1 cm were used as substrates for all experiments. Fifty of these conducting glasses were drilled with two holes to serve as counter electrodes. Prior to use, all substrates underwent a comprehensive cleaning procedure to remove contaminants. Initial cleaning involved gently scrubbing the substrate surfaces with cotton swabs dipped in a solution containing sodium hydroxide, detergent (Helmanex soap), and deionized water. The substrates were then thoroughly rinsed with deionized water. Further cleaning was performed to remove specific contaminants such as oils and organic residues using acetone and absolute ethanol (both purchased from Sigma-Aldrich). Since acetone can leave residues on substrate surfaces, a two-solvent cleaning protocol was employed for thorough decontamination. The cleaning process involved sequential ultrasonic agitation (model: LUC-405) for 15 minutes at each solvent step: The substrates were first soaked in acetone and agitated ultrasonically for 15 minutes to remove organic contaminants. Then the substrates were soaked in ethanol and agitated for another 15 minutes to remove acetone residues, and finally the substrates were soaked in deionised water and agitated for 15 minutes to ensure complete removal of all residues After air drying for 30 minutes, the substrates were finally cleaned using an Ossila UV ozone cleaner for 10 minutes.

2.2.2 Spray Pyrolysis for Compact Layer Deposition

Fifteen cleaned glass substrates were selected for compact layer deposition. A 1 cm $\times$ 1 cm area was marked on each substrate as the active area for solar cell preparation. The precursor solution was prepared by mixing three reagents: titanium diisopropoxide bis(acetylacetonate) (75 wt.% in isopropanol, Sigma-Aldrich), acetylacetone (Merck), and ethanol (Sigma-Aldrich). The preparation process involved: Measuring 9.0 mL of ethanol into a beaker, adding 0.4 mL of acetylacetone, adding 0.6 mL of titanium diisopropoxide, and then stirring the mixture using a magnetic stirrer (model: CB 162) at a constant temperature of 30°C to create a stable, soluble precursor solution The precursor solution was deposited onto the cleaned FTO glass substrates using a spray pyrolysis system (model: HO-TH-04) equipped with an ultrasonic spray head. The deposition was performed in vertical geometry with the following parameters: Ultrasonic atomization speed: 25 m/s, frequency: 40 kHz, carrier gas: compressed air at 2 bar pressure, solution flow rate: 2 mL/min, deposition time: 60 seconds, nozzle-to-substrate distance: 15 cm and then the substrate temperature: 450°C. After compact layer preparation, one FTO substrate was reserved for film thickness testing, while the remaining substrates were used for subsequent TiO_2 film deposition.

2.2.3 Preparation of the Titanium Dioxide Layer

A commercially available titanium dioxide paste (Sigma-Aldrich, titanium paste transparent: mkcr1436) was used for TiO_2 layer deposition. The paste was deposited directly onto the predetermined area above the compact layer, creating a bilayer structure consisting of the compact layer and TiO_2 nanoparticle layer. The TiO_2 nanoparticle layer was deposited using spin coating (model: P6708D) with the following parameters: Rotation speed of 4000 rpm and a duration of 2 minutes. After deposition, areas outside the predetermined region were cleaned using cotton swabs, and the deposited film was dried on a heat block for 10 minutes at 120°C. This process yielded fourteen samples. The substrates were subsequently annealed in a tube furnace at 450°C with stepwise temperature increments for one hour, followed by gradual cooling. Two samples were reserved for thickness testing.

2.2.4 Dye Preparation

Both commercial synthetic dye and natural dyes extracted from *Spinacia oleracea* (spinach leaves) and *Bougainvillea glabra* (bougainvillea flowers) were prepared. These plant materials were selected due to their ready availability, lack of seasonal dependency, and presence of required pigments (chlorophyll and anthocyanin).

Synthetic Dye Preparation A ruthenium dye (N-719, Solaronix Ruthenienizer 535-bis TBA, BN P266/200924) solution was prepared by dissolving 6 mg of Ru-719 in 10 mL of ethanol to create a 0.5 mM solution. The solution was thoroughly mixed to ensure that it had dissolved uniformly.

Natural Dye Extraction Spinach was purchased from Quickmart supermarket, while bougainvillea flowers were harvested at Jomo Kenyatta International Airport main entrance (coordinates: -1.3476519, 36.9041115). The extraction process involved: Cleaning: Plant materials were washed with deionized water to remove dust and contaminants, followed by sequential cleaning with acetone and ethanol, and final rinsing with deionized water, drying: Materials were air-dried in a dark room with free air circulation for 12 hours, and Extraction: 150 g of each dried sample was weighed using an analytical balance (model: ATY 224 R). Spinach leaves were ground with 450 mL of ethanol until a fine solution was obtained, then filtered using filter paper D 42. The same process was repeated for bougainvillea flowers. The two extracted solutions were mixed at room temperature in different concentration ratios of chlorophyll to anthocyanin: 100%:0%, 90%:10%, 80%:20%, 70%:30%, 60%:40%, 50%:50%, 40%:60%, 30%:70%, 20%:80%, 10%:90%, and 0%:100% respectively. Half of each prepared mixture was reserved for optical analysis using a Shimadzu UV-VIS spectrophotometer (model: Solid Spec-3700 DUV). Eleven prepared TiO_2 thin film substrates were soaked in the dye mixtures for 24 hours in a dark room covered with aluminum foil. One additional substrate was soaked in the ruthenium dye solution under identical conditions. All substrates were maintained at room temperature during the sensitization process.

2.2.5 Determination of Dye Concentration

Dye concentrations were determined using Beer-Lambert's law, which relates absorption magnitude directly to solution concentration. The analysis focused on absorption values within the visible range region. A known concentration ruthenium dye solution (0.5 mM) was used as the standard and diluted to create solutions of 0.25 mM and 0.125 mM concentrations using the relationship $C_1V_1 = C_2V_2$. Each concentration sample was analyzed to establish a calibration curve for determining unknown dye concentrations.

2.2.6 Counter Electrode Preparation

Pre-drilled counter electrodes were cleaned following the same procedure as the photoanodes until completely clean and dry. Platinum solution (Platisol T/SP, Solaronix SA, Switzerland) was coated onto the conductive side of the cleaned FTO glass substrates and heated in a tube furnace with stepwise temperature increase to 450°C for 30 minutes. The counter electrodes were then allowed to cool slowly before use.

2.2.7 Solar Cell Assembly

After 24 hours of dye sensitization, the substrates were retrieved and rinsed in ethanol to remove excess dye. They were dried on a hot plate for 10 minutes at 70°C while being properly labeled. The solar cells were assembled by fusing the photoelectrodes with counter electrodes in a sandwich

configuration using a 60 μm thick thermoplastic sealing gasket made of Surlyn (Solaronix, Switzerland). The assembly was performed under slight mechanical pressure at 100°C. An iodide/tri-iodide electrolyte was introduced into the assembled solar cells through one of the holes in the counter electrode using a vac 'n' fill syringe. Excess electrolyte was removed by wiping, and the cells were prepared for I-V characterization.

2.2.8 Current-Voltage (I-V) Characterization of Solar Cells

Current-voltage characterization was performed using an Ossila solar simulator equipped with an AM filter and a source meter controlled by computer. The system employs a xenon arc lamp that emits a light spectrum similar to sunlight. The light is conditioned using optical components including lenses, mirrors, and filters to achieve the desired intensity, uniformity, and spectral distribution. The solar simulator connects to a computer via USB cable for data collection and analysis using solar simulator console software to determine solar cell performance. Measurements were conducted under standard test conditions with an illumination intensity of 100 mW/cm^2 (1000 W/m^2) at the solar cell surface. Parameters obtained from the characterization included fill factor (FF), short-circuit current density (J_{sc}), open-circuit voltage (V_{oc}), and maximum power (p_{max}. Power conversion efficiency was calculated from these parameters.

3 Results and Discussion

3.1 Dye Extraction and Mixing

Chlorophyll and anthocyanin dye solutions were successfully extracted through solvent extraction as described in section 2.2.4. The extracted dyes were filtered to obtain clear solutions free from sediments. Subsequently, the chlorophyll and anthocyanin dyes were mixed in various percentage ratios ranging from pure chlorophyll (100%:0%) to pure anthocyanin (0%:100%), creating eleven distinct dye mixtures for analysis.

The dye mixtures were prepared according to the ratios shown in Table 1, with each sample containing a total volume of 10 mL. This systematic approach allowed for comprehensive analysis of the optical properties across the full spectrum of chlorophyll-anthocyanin combinations.

Table 1: **Chlorophyll and anthocyanin mixture compositions**

Sample number (S)	S_A	S_B	S_C	S_D	S_E	S_F	S_G	S_H	S_I	S_J	S_K
Chlorophyll (mL)	10	9	8	7	6	5	4	3	2	1	0
Anthocyanin (mL)	0	1	2	3	4	5	6	7	8	9	10
Ratio	10:0	9:1	8:2	7:3	6:4	5:5	4:6	3:7	2:8	1:9	0:10
Percentage ratio (%)	100:0	90:10	80:20	70:30	60:40	50:50	40:60	30:70	20:80	10:90	0:100

3.2 Confirmation of Chlorophyll and Anthocyanin Presence

The plant materials were analyzed to confirm the presence of the required pigments. Chlorophyll, predominantly found in green plant parts, was extracted from *Spinacia oleracea* (spinach leaves). Anthocyanin, typically present in colored plant parts such as fruits and flowers exhibiting red, purple, and blue hues, was extracted from *Bougainvillea glabra* (red bougainvillea flowers).

UV-VIS spectrophotometric analysis was performed to determine the absorption peaks of both extracted dyes within the visible light region (400–780 nm). The results confirmed the presence of the target pigments based on their characteristic absorption patterns.

Chlorophyll exhibited a broad absorption peak within the visible light region from 400 nm to approximately 450 nm, followed by a gradual decline in absorption. Similarly, anthocyanin demonstrated a wide absorption range from 400 nm to approximately 580 nm, after which absorption gradually decreased. These absorption characteristics are consistent with literature values, confirming successful extraction of chlorophyll (peak around 450 nm) and anthocyanin (peak around 580 nm) from the selected plant materials.

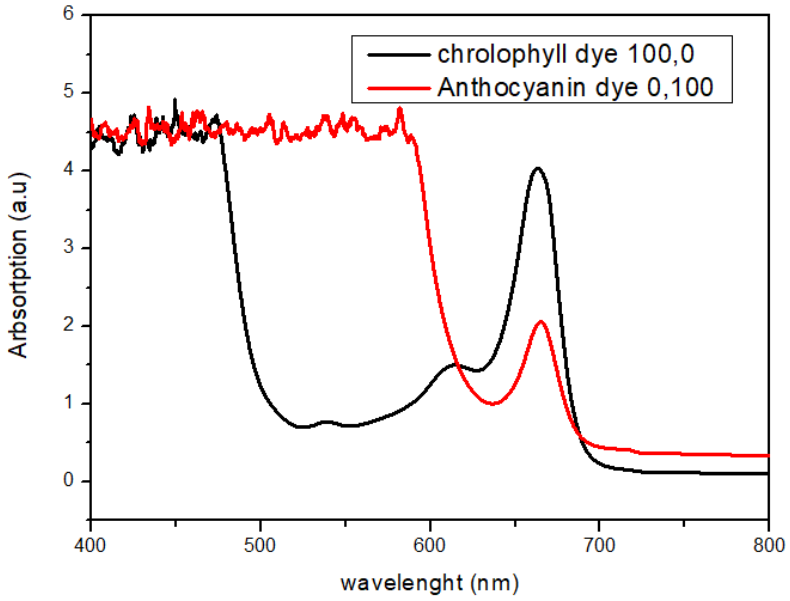

Figure 1: **Absorption spectra showing chlorophyll and anthocyanin absorption ranges**

3.3 Determination of Chlorophyll and Anthocyanin Concentrations

The concentrations of the extracted dyes were determined using Beer-Lambert law, which establishes a direct relationship between absorbance and concentration. A standard ruthenium dye solution (0.5 mM) was used as the reference and diluted to create calibration standards of 0.25 mM and 0.125 mM concentrations using the dilution equation:

$$C_1V_1 = C_2V_2 \tag{3.1}$$

The absorbance measurements were conducted at the wavelength of maximum absorption within the visible region. Beer-Lambert law relates concentration to absorbance according to:

$$C = \frac{A}{\epsilon L} \tag{3.2}$$

where C is concentration, A is absorbance, ϵ is molar absorptivity of the dye, and L is path length.

For the ruthenium dye standards, the highest absorbance values were identified at 437 nm. Consequently, the unknown dye concentrations were determined by measuring their absorbance at the same wavelength using identical blank solutions.

Table 2: **Ruthenium dye calibration data at 437 nm**

Known solution	Wavelength (nm)	Absorbance (a.u.)	Concentration (mM)
Ruthenium dye	437	1.358	0.125
Ruthenium dye	437	2.740	0.250
Ruthenium dye	437	5.467	0.500

A calibration curve was constructed from the data in Table 2, establishing a linear relationship between concentration and absorbance. This calibration curve was subsequently used to determine the concentrations of the extracted chlorophyll and anthocyanin dyes. From figure 1, of the absorbance peaks of chlorophyll and anthocyanin, the recorded absorbances at the maximum wavelength 437 were determined as 4.921 and 4.820 a.u, respectively.

Using the linear equation derived from the calibration curve shown in Figure 2, the concentrations of the extracted natural dyes were calculated and are presented in Table 3.

Table 3: **Concentration determination of extracted natural dyes at 437 nm**

Unknown solution	Wavelength (nm)	Absorbance (a.u.)	Concentration (mM)
Chlorophyll dye	437	4.921	0.450
Anthocyanin dye	437	4.820	0.441

The results indicate that both extracted dyes achieved concentrations comparable to the ruthenium standard, with chlorophyll at 0.450 mM and anthocyanin at 0.441 mM. These concentrations are suitable for dye-sensitized solar cell applications.

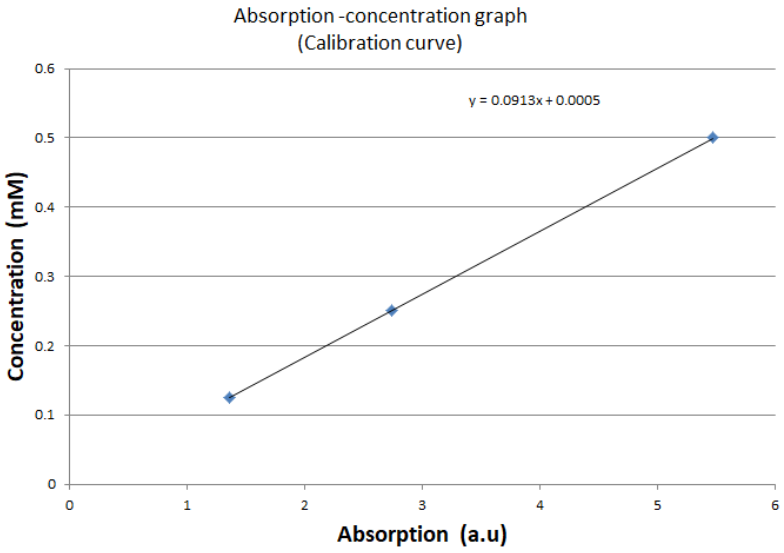

Figure 2: **Ruthenium dye concentration calibration curve**

3.4 Optical Analysis of Dye Mixtures

The prepared dye mixtures underwent comprehensive optical characterization using UV-VIS spectrophotometry to evaluate their transmittance and absorption properties across the visible spectrum.

3.4.1 Transmittance Analysis

Figure 3 presents the transmittance spectra of all dye mixtures compared to the commercial ruthenium complex dye. The analysis reveals that all tested dyes exhibit minimal transmittance within the visible light region of 0.0001%. This is determined from the absorption graph, figure 4, where the highest absorbance is 6 a.u. Conversion of this to percentage transmittance by formula T% = 10^{2-A} , which is a desirable property for effective light harvesting in photovoltaic applications.

The transmittance analysis demonstrates that the ruthenium dye exhibited the lowest transmittance values, indicating superior light-blocking capability within the visible spectrum. This characteristic contributes to more efficient light trapping and energy conversion. The natural dye mixtures also showed low transmittance values, suggesting their potential effectiveness as light-harvesting sensitizers in solar cell applications.

The systematic variation in dye composition from pure chlorophyll to pure anthocyanin provides insight into how the optical properties change with mixture ratio, enabling optimization of the dye composition for enhanced solar cell performance.

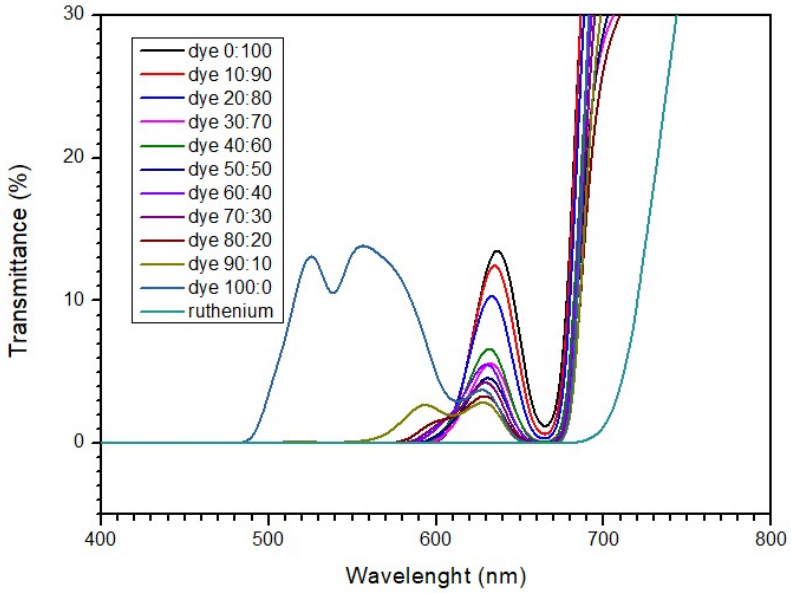

Figure 3: **Transmittance spectra comparison of ruthenium, chlorophyll, anthocyanin, and their mixtures**

3.4.2 Dye Absorption Curves

UV-VIS spectrophotometer was used in dye absorption analysis. The figure 4 show the absorption criteria for different mixtures. Mixing chlorophyll and anthocyanin increases the range of light absorption. This mainly happen because each pigment absorbs different wavelength of the visible light region thus when all combined together they effectively capture a wide spectrum of light essentially by “filling in the gaps” between the wavelengths where each pigment absorbs individually. This results in a broadening absorption range cross the visible light spectrum.

Analysis of each percentage mixing has attributed to unique results and trends. From figure 4, anthocyanin shows that it has better absorption of around 400–580 nm range than chlorophyll which have an absorption range of 400–450 nm. Thus, mixing chlorophyll and anthocyanin resulted to an improvement of chlorophyll’s capacity to absorb light.

The higher the concentration of anthocyanin in a mixture, it broadens the absorption spectrum range of the mixture within the visible range, thus boosting chlorophyll absorption capacity in the mixture.

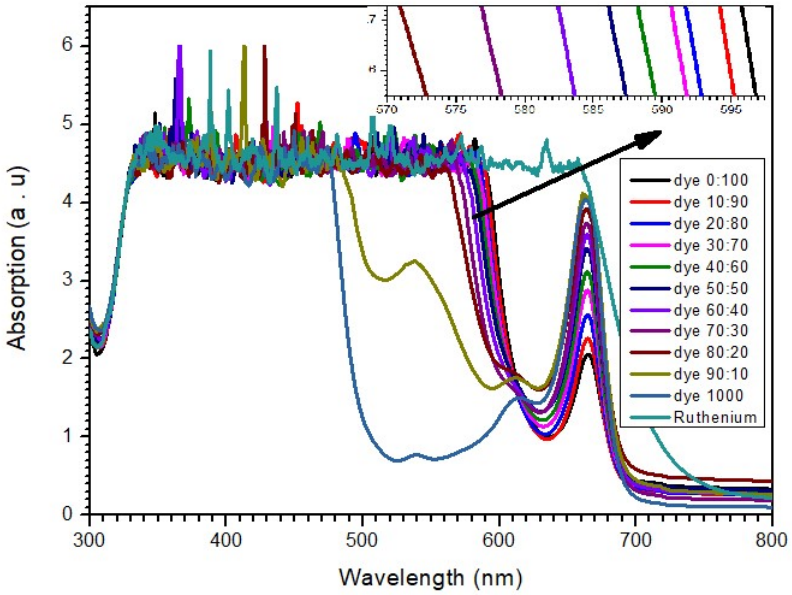

Figure 4: **Absorbance graph for ruthenium, chlorophyll, anthocyanin and their mixtures**

3.4.3 Optical Characterisation of Annealed Thin Film

Transmittance spectra for the two-layer and annealed TiO_2 films displayed a gradual increase in transmittance as wavelength increases from 350–400 nm as shown in the figure 5. This indicates that visible light (400-700 nm) transmits very well through the film which is an excellent feature for solar cells in harvesting visible light from sun.

Transmittance decreases with increase of the number of films with one film being more transparent than two layer film. This is the expected observation based on Beer-Lambert law equation as shown:

$$A = -\log_{10}\left(\frac{I}{I_0}\right)$$

Where A is the absorbance, I_0 is the incident intensity and I the transmitted intensity.

Analysis for energy absorption for the two layer compact layer and TiO_2 was analyzed as shown in the figure 6:

From figure 6, the absorption was analyzed to indicate that absorption was minimal within the visible region meaning that the light penetrated the two layers at ease. The graph analysis was used to determine the band gap of the thin film deposited at room temperature.

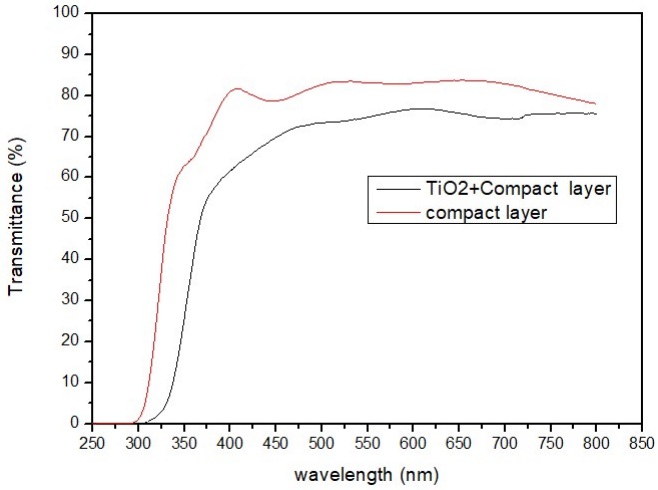

Figure 5: **Compact layer and TiO_2 Film transmittance graph**

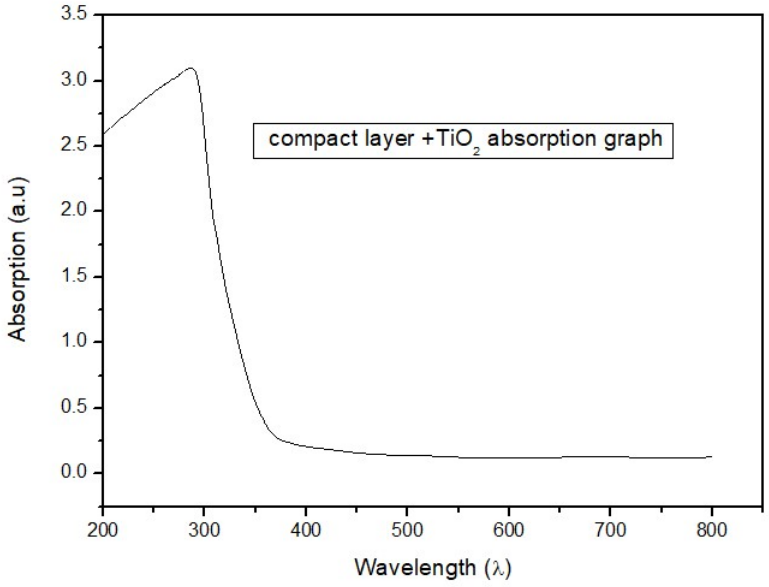

Figure 6: **Compact layer + TiO_2 Film absorption graph**

The figure 7 depicts the transmittance of a material as light passes through it, which enables the calculation of energy-gap of a material using Tauc's plot method started by calculating the absorption coefficient (α). The absorption coefficient is given by the Beer-Lamberts law:

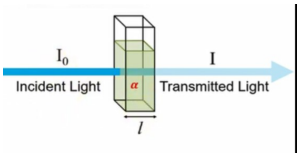

Figure 7: **The absorption and transmittance of light by a sample**

I = $I_0 e^{-\alpha\chi}$,
$\frac{I}{I_0} = e^{-\alpha\chi}$,
$\log \frac{I}{I_0} = \log e^{-\alpha\chi}$,
$\log \frac{I}{I_0} = -\alpha\chi \log e$,
$\log \frac{I_0}{I} = \alpha\chi \log e$,
$A = \alpha\chi \log e$,
where $\log e = 0.4343$,
$\alpha = (2.3025)\frac{A}{\chi}$ (3.3)

Where: A is absorbance value from UV – VIS spectrophotometer
That wavelength was converted to energy as follows:

$$E = hv = h\frac{c}{\lambda} \tag{3.4}$$

Where:

- E is energy,
- h is Planck's constant,
- c is speed of light,
- λ is wavelength.

Absorption values at different wavelengths were plotted in Tauc graph using:

$$(\alpha hv)^{1/\gamma} = B(hv - E_g) \tag{3.5}$$

Where:

- α is the absorption coefficient,
- h Planck's constant,
- v is frequency of photon,
- E_g is energy gap,
- B is a proportionality constant (assumed 1),
- γ is transition type:
    1. $\frac{1}{2}$ for direct transition,
    2. 2 for indirect transition.

The figure 8 obtained from the two layer film indicates that the energy gap of the film is around 3.18 eV, which is close to the well-known TiO_2 band gap of 3.2 eV (direct transition).

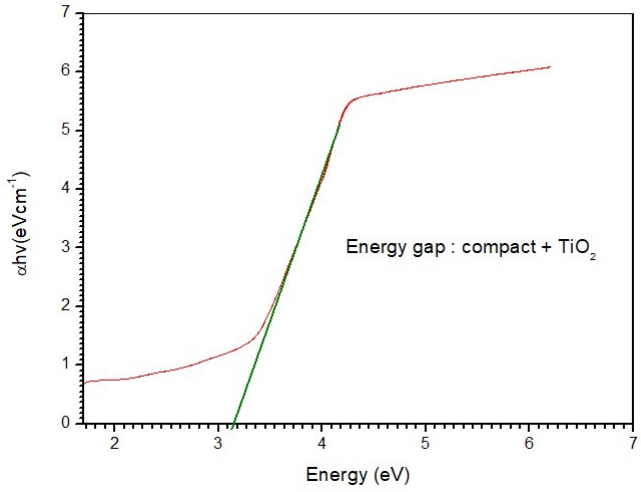

Figure 8: **Energy gaps graph**

3.4.4 Film Thickness of Annealed Compact and TiO_2 Layer

The two layers' profile was determined using a DEKTAK Profilometer. The films covered an area of $1\,\text{cm} \times 1\,\text{cm}$ on the glass substrate. The table below summarizes the thickness test performed. These were the values obtained after measuring varying film thicknesses:

Table 4: **Thickness analysis**

Trial No.	Compact Layer Thickness (μm)	TiO_2 Layer Thickness (μm)	Compact + TiO_2 Layer Thickness (μm)
1	5.4	13.0	19.9
2	6.2	14.4	20.0
3	5.9	13.7	20.2
4	5.7	13.4	19.6
5	6.7	14.4	18.9
Average	**6.0**	**13.8**	**19.7**

3.4.5 Compact Layer Size and Functionality

After thickness testing, the compact layer showed a thickness of around 6.0 μm. The compact layer helps DSSCs by blocking excited electrons from recombination. This reduces recombination losses, shifts the Fermi level upward, and increases electron concentration—resulting in higher current density. Furthermore, it enhances interfacial adhesion between the nanoporous TiO_2 and the substrate, thus improving the fill factor and cell stability.

3.4.6 Current–Voltage (I–V) Characteristics

Chlorophyll and anthocyanin dyes were mixed to improve DSSCs' ability to harvest visible light. I–V characterization was conducted at room temperature under illumination intensity of 100 $\text{mW}\cdot\text{cm}^{-2}$.

Ethanol was used as the solvent for dye extraction, and different mixing ratios were prepared. From figure 9, the standard ruthenium dye exhibited the best performance. Table 5 summarizes their photovoltaic parameters:

Table 5: **Natural dye mixtures' efficiency**

Dye mixture (%)	V_{oc} (V)	J_{sc} ()	Fill factor (FF)	η (%)
0:100	0.585	1.02	0.620	0.37
10:90	0.580	0.98	0.619	0.35
20:80	0.570	0.92	0.608	0.32
30:70	0.550	0.89	0.539	0.26
40:60	0.545	0.81	0.542	0.24
50:50	0.530	0.69	0.564	0.21
60:40	0.520	0.59	0.538	0.17
70:30	0.500	0.51	0.587	0.15
80:20	0.495	0.47	0.563	0.13
90:10	0.485	0.40	0.558	0.11
100:0	0.460	0.34	0.519	0.08
Ruthenium (N-719)	0.640	11.8	0.673	5.08

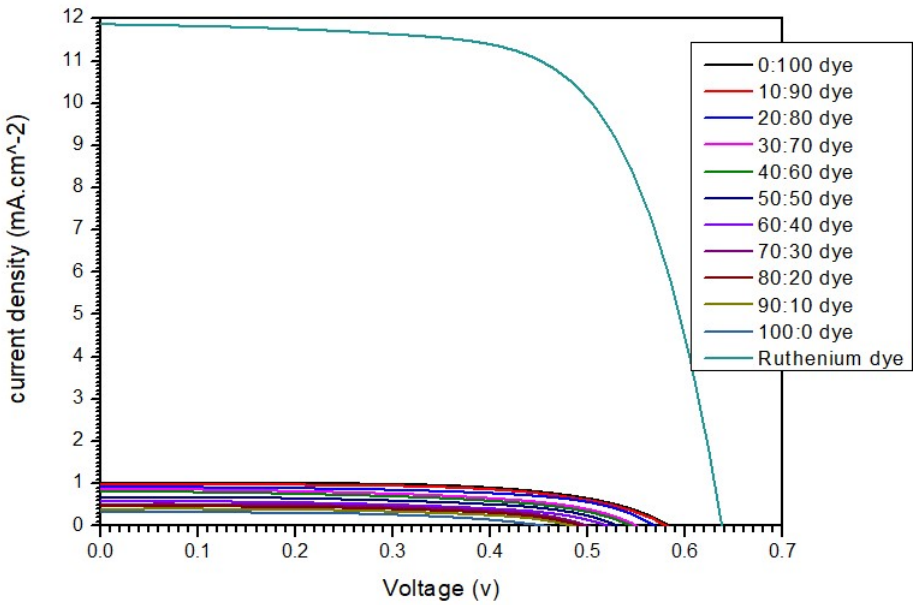

Figure 9: **I–V curves for standard ruthenium dye and natural dye mixtures**

From figure 10, the pure anthocyanin (0:100) dye exhibited the highest performance among natural dye mixtures due to its wide absorption spectrum. This was followed by mixtures with higher anthocyanin content. The trend in efficiency was: 0:100, 10:90, 20:80, ..., down to 100:0.

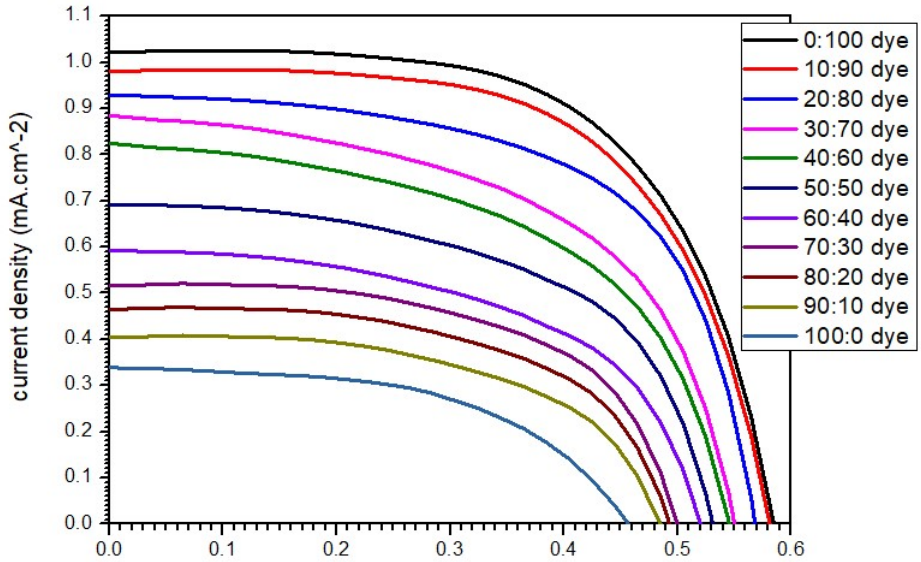

Figure 10: **I–V curves for natural dye mixtures**

Chlorophyll-only (100:0) showed the lowest efficiency, consistent with its narrower absorption range. Thus, mixing with anthocyanin improves the overall performance of chlorophyll dyes by broadening the light absorption spectrum.

4 CONCLUSIONS

a In the section (3.1), Dye sample solutions of chlorophyll and anthocyanin were extracted via solvent extraction, filtered and then mixed in different ratios of 100%:0%, 90%:10%, 80%:20%, 70%:30%, 60%:40%, 50%:50%, 40%:60%, 30%:70%, 20%:80%, 10%:90% and 0%:100% respectively.

b In the subsection (3.2), the plant products used were analyzed to check if they had the required pigments (chlorophyll and anthocyanin).

c In the subsection (3.3), the dillution of the known concentrated dye to different solutions concentrations was done and their absorbance characteristic determined. Where the absorbance data of the ruthenium dyes showed the highest absorbance values within the visible light region at 437 nm, and the absorbance of the unknown solutions was determined at the same wavelength of 437 nm.

d In the subsections (3.4.2 and 3.4.1), he transmittance of the dye mixtures in reference to standard solution of commercial ruthenium complex dye was determined, where ruthenium had the least transmittance indicating that, it permits less amount of light to penetrate past the dye within the visible light region. futhermore, the dye absorption curves were determined by the UV-VIS spectrophotometer, which showed that mixing chlorophyll and anthocyanin increases the range of light absorption.

e In the subsection (3.4.3), the optical characterization of the annealed thin films was done, and the transmittance spectra for the two layer and annealed TiO_2 films displayed a gradual increase in transmittance as wavelength increases indicating that visible light transmits very well through the film which is an excellent feature for solar cells in harvesting visible light from sun. This was used to calculate the Beer-Lambert's law.

f In the subsection (3.4.4), the film thickness of annealed compact and TiO_2 layer were determined using a DEKTAK- Profilometer.

g In the subsection (3.4.5), Compact layer size and its effect on the functionality of the DSSC was determined.

h In the subsection (3.4.6), Current-voltage (I-V) Characteristics of the DSSC were determined at room temperature, with the aim of determining effects of Chlorophyll and anthocyanin dyes on the DSSC's ability to harvest visible light. It was found out that pure anthocyanin dye led to higher efficiency compared to all other dyes since it has a wider spectrum range for absorbing visible light and chlorophyll had the lowest absorption spectrum range of visible light hence the lowest cell efficiency. Futhermore, mixtures' efficiencies depend on the amount of anthocyanin present, and thus higher quantity of anthocyanin leads to higher efficiency compared to chlorophyll.

.

References

Muñoz-García, A. B., Benesperi, I., Boschloo, G., Concepcion, J. J., Delcamp, J. H., Gibson, E. A., Meyer, G. J., Pavone, M., Pettersson, H., Hagfeldt, A., & Freitag, M. (2021). Dye-sensitized solar cells strike back. *Chemical Society Reviews*. https://doi.org/10.1039/d0cs01336f

Sekaran, P. D., & Marimuthu, R. (2024). An extensive analysis of dye-sensitized solar cell (dssc). *Brazilian Journal of Physics*, *54*(1), 28.

Sugathan, V., John, E., & Sudhakar, K. (2015). Recent improvements in dye sensitized solar cells: A review. *Renewable and Sustainable Energy Reviews*, *52*, 54–64.

Badawy, S. A., Abdel-Latif, E., & Elmorsy, M. R. (2024). Tandem dye-sensitized solar cells achieve 12.89% efficiency using novel organic sensitizers. *Scientific Reports*, *14*(1), 26072.

Parasuraman, D., & Ramakrishnan, M. (2023). A review on dye-sensitized solar cells (dsscs), materials and applications. *Iranian Journal of Materials Science & Engineering*, *20*(1).

Saud, P. S., Bist, A., Kim, A. A., Yousef, A., Abutaleb, A., Park, M., Park, S.-J., & Pant, B. (2024). Dye-sensitized solar cells: Fundamentals, recent progress, and optoelectrical properties improvement strategies. *Optical Materials*, *150*, 115242.

Lin, S., He, X., Xu, Q., Li, Y., & Fang, D. (2025). Research progress on dyes for n-type dye-sensitized solar cells. *Materials Science and Engineering: B*, *314*, 118052.

Khan, M., Iqbal, M. A., Malik, M., Hashmi, S. U. M., Bakhsh, S., Sohail, M., Qamar, M. T., Al-Bahrani, M., Capangpangan, R. Y., Alguno, A. C., et al. (2023). Improving the efficiency of dye-sensitized solar cells based on rare-earth metal modified bismuth ferrites. *Scientific Reports*, *13*(1), 3123.

Kokkonen, M., Talebi, P., Zhou, J., Asgari, S., Soomro, S., Elsehrawy, F., et al. (2021). Advanced research trends in dye-sensitized solar cells. *Journal of Materials Chemistry A*, *9*(17), 10527–10545. https://doi.org/10.1039/D1TA01277K

Iqbal, M. Z., Ali, S. R., & Khan, S. (2019). Progress in dye sensitized solar cell by incorporating natural photosensitizers. *Solar Energy*, *181*, 490–509.

Pirdaus, N. A., Ahmad, N., Muhammad-Sukki, F., & Wan-Mohtar, W. A. A. Q. I. (2024). A narrative review on vital criteria of fungal dyes as dye-sensitized solar cell (dssc). *Discover Applied Sciences*, *6*(10), 553.